

This author's accepted manuscript may be used for non-commercial purposes in accordance with [Wiley Terms and Conditions for Self-Archiving](#).

The full details of the published version of the article are as follows:

TITLE: Integrating morphology and in vivo skeletal mobility with digital models to infer function in brittle star arms

AUTHORS: Elizabeth G. Clark, John R. Hutchinson, Simon A. F. Darroch, Nicolás Mongiardino Koch, Travis R. Brady, Sloane A. Smith, Derek E. G. Briggs

JOURNAL: Journal of Anatomy

PUBLISHER: Wiley

PUBLICATION DATE: 23 October 2018 (online)

DOI: <https://doi.org/10.1111/joa.12887>

Integrating morphology and in vivo skeletal mobility with digital models to infer function in brittle star arms

Elizabeth G. Clark,¹ John R. Hutchinson,² Simon A. F. Darroch,³ Nicol as Mongiardino Koch,¹ Travis R. Brady,⁴ Sloane A. Smith⁴ and Derek E. G. Briggs^{1,5}

¹Department of Geology and Geophysics, Yale University, New Haven, CT, USA

²Structure and Motion Laboratory, Department of Comparative Biomedical Sciences, The Royal Veterinary College, Hertfordshire, UK

³Department of Earth and Environmental Science, Vanderbilt University, Nashville, TN, USA

⁴Department of Biomedical Engineering, Yale University, New Haven, CT, USA

⁵Yale Peabody Museum of Natural History, Yale University, New Haven, CT, USA

Abstract

Brittle stars (Phylum Echinodermata, Class Ophiuroidea) have evolved rapid locomotion employing muscle and skeletal elements within their (usually) five arms to apply forces in a manner analogous to that of vertebrates. Inferring the inner workings of the arm has been difficult as the skeleton is internal and many of the ossicles are sub-millimeter in size. Advances in 3D visualization and technology have made the study of movement in ophiuroids possible. We developed six virtual 3D skeletal models to demonstrate the potential range of motion of the main arm ossicles, known as vertebrae, and six virtual 3D skeletal models of non-vertebral ossicles. These models revealed the joint center and relative position of the arm ossicles during near-maximal range of motion. The models also provide a platform for the comparative evaluation of functional capabilities between disparate ophiuroid arm morphologies. We made observations on specimens of *Ophioderma brevispina* and *Ophiothrix angulata*. As these two taxa exemplify two major morphological categories of ophiuroid vertebrae, they provide a basis for an initial assessment of the functional consequences of these disparate vertebral morphologies. These models suggest potential differences in the structure of the intervertebral articulations in these two species, implying disparities in arm flexion mechanics. We also evaluated the differences in the range of motion between segments in the proximal and distal halves of the arm length in a specimen of *O. brevispina*, and found that the morphology of vertebrae in the distal portion of the arm allows for higher mobility than in the proximal portion. Our models of non-vertebral ossicles show that they rotate further in the direction of movement than the vertebrae themselves in order to accommodate arm flexion. These findings raise doubts over previous hypotheses regarding the functional consequences of ophiuroid arm disparity. Our study demonstrates the value of integrating experimental data and visualization of articulated structures when making functional interpretations instead of relying on observations of vertebral or segmental morphology alone. This methodological framework can be applied to other ophiuroid taxa to enable comparative functional analyses. It will also facilitate biomechanical analyses of other invertebrate groups to illuminate how appendage or locomotor function evolved.

Key words: 3D digital modeling; locomotion; mobility; Ophiuroidea; range of motion.

Introduction

Deuterostomia, the superphylum containing chordates, hemichordates and echinoderms, includes more than 66 000 species and a multitude of disparate body plans (Brusca & Brusca, 1990; Lake, 1990; Halanych, 2004; Bisby et al. 2010; Edgecombe et al. 2011). Even within this diversity, many deuterostomes have an internal hard skeleton that,

1 when acted on by muscles, allows for a variety of motions,
2 permitting these organisms to run, swim and fly. Extensive
3 biomechanical research has been conducted on motion in
4 chordates, in particular vertebrates (Leach & Dagg, 1983;
5 Alexander, 1992a,b, 2003; Bels et al. 2003). However, muscle
6 physiology and mechanical properties of the other major
7 deuterostome clade, the echinoderms, is much less well
8 known. Study of this group is critical to obtaining a deeper
9 picture of the evolution of deuterostome locomotion.

10 The phylum Echinodermata includes an estimated 13 000
11 extinct and 7000 extant species (Pawson, 2007), the latter
12 representing five body plans: crinoids (class Crinoidea); sea
13 stars (class Asteroidea); sea cucumbers (class Holothuroidea);
14 sea urchins (class Echinoidea); and brittle stars (class Ophi-
15 uroidea). The five living echinoderm classes each employ a
16 unique locomotion strategy (and additional locomotion
17 strategies were presumably used by extinct echinoderm
18 classes). Crinoids, although typically sessile, can crawl or
19 swim using their many arms (Moore, 1924; Shaw & Fon-
20 taine, 1990; Baumiller & Messing, 2007). Sea stars use water
21 pressure to control tube feet to move themselves across the
22 ocean floor (Smith, 1947; Kerkut, 1953). Sea cucumbers gen-
23 erally crawl or burrow using wave-like body movements
24 (Glynn, 1965), but certain forms can walk using modified
25 tube feet (Hansen, 1972; Gebruk, 1995) or swim (Glynn,
26 1965; Ohta, 1985; Gebruk, 1995). Sea urchins move using a
27 combination of tube feet and muscle-actuated spines
28 (Domenici et al. 2003). These four extant classes are typically
29 slow moving as they generally do not rely on rapid locomo-
30 tion for survival.

31 Many extant ophiuroids, in contrast, coordinate move-
32 ments in each of their (usually) five arms to produce rela-
33 tively rapid locomotion. Their arms consist of modular
34 segments (sometimes more than 100 per arm; LeClair, 1996)
35 composed of skeletal elements (ossicles), which are joined
36 via connective tissue and muscle. Connective tissue between
37 successive ossicles is made of specialized material that can
38 change its tensile stiffness and strength under nervous con-
39 trol (Wilkie, 1978a, 2005). Arm segments are typically com-
40 posed of five internal ossicles: a vertebra and a dorsal,
41 ventral and two lateral plates (laterals; Fig. 1). The vertebral
42 ossicles are the most critical for movement as they incorpo-
43 rate the intervertebral muscle attachments and joint inter-
44 faces. Four intervertebral muscles, two aboral and two oral,
45 attach to each vertebra surrounding a central intervertebral
46 joint (Wilkie, 1978b; Byrne, 1994; Clark et al. 2017). Con-
47 traction of the intervertebral muscles allows the distal of the
48 two segments to pivot around the joint (LeClair, 1996). A
49 series of spines extends from the laterals, varying in thick-
50 ness, length and number between species.

51 The ophiuroid fossil record dates back to the Ordovician
52 (Shackleton, 2005), but the crown group did not evolve
53 until the Late Paleozoic (O'Hara et al. 2014). Although
54 superficially similar, there are distinct morphological differ-
55 ences between stem and crown ophiuroids, particularly in

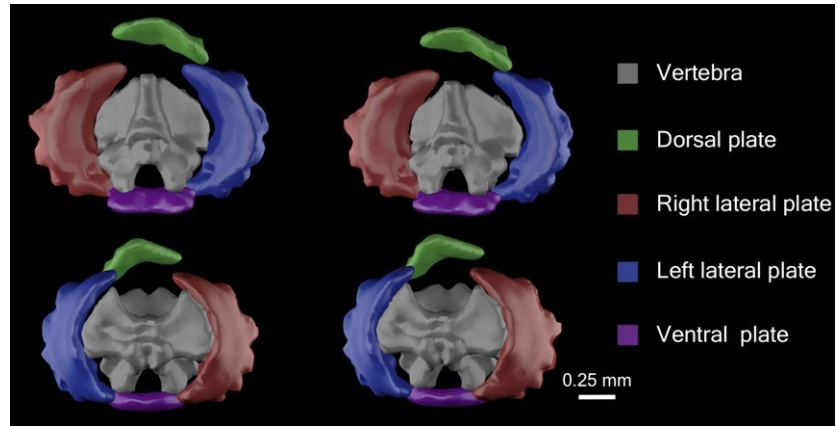
the arms. Specifically, they generally differ in the ossicles
that run along the axis of the arm. Modern ophiuroids have
one massive vertebra at the center of each segment. Many
Paleozoic forms, in contrast, have two sets of small ossicles
(ambulacra) through the center of the arm resembling a
zipper, and the morphology of these small ossicles differs
among Paleozoic taxa. Paired, fused ambulacra are hypoth-
esized to be an autapomorphy of crown group ophiuroids
(Smith et al. 1995). Most Paleozoic taxa lack dorsal and ven-
tral plates. The functional capabilities of these fossil ossicle
arrangements are largely unknown.

During locomotion of modern ophiuroids, each arm
performs a series of repetitive actions depending on its
position relative to the direction of motion. These actions
are redistributed during direction changes so that the
organism can move omnidirectionally without turning
the central disk (Astley, 2012; Kano et al. 2012; Mao
et al. 2014). Ophiuroids adjust the actions performed by
the arms in response to arm damage or loss to minimize
decrease in movement capability, and they can continue
locomotion using tube feet on the ventral surface of the
disk even when all the arms are removed (Arshavskii
et al. 1976a; Kano et al. 2017; Matsuzaka et al. 2017).
They coordinate arm movements using decentralized con-
trol (Kano et al. 2012, 2017; Watanabe et al. 2012). Fea-
tures of ophiuroid arms and locomotion have been
applied to robotics (Lal et al. 2008; Kano et al. 2012,
2017; Watanabe et al. 2012; Mao et al. 2014), biomaterial
development (Wilt, 2005; Barbaglio et al. 2012, 2013) and
regenerative medicine (Dupont & Thorndyke, 2007; Can-
dia Carnevali & Burighel, 2010; Green et al. 2016).

Despite these powerful applications and the unique na-
ture of ophiuroid locomotion, it has been the subject of rela-
tively little experimental research, in particular on how
ossicle morphology and articulation influence range of
motion. The gait patterns of ophiuroid arms (i.e. the differ-
ent distributions of rhythmic coordinated actions of the
arms to produce locomotion) have been studied (Arshavskii
et al. 1976a,b; Astley, 2012; Watanabe et al. 2012; Kano
et al. 2017; Matsuzaka et al. 2017), and ranges of lateral
motion in the arms have been measured externally on living
specimens (LeClair & LaBarbera, 1997). However, it has been
difficult to infer the functions of the arm joints in an
anatomical context, due to their small size and because the
key areas of interest are obscured by soft tissue and ossicles
(Fig. 1).

There are two joint morphologies, streptospondylous and
zygospondylous, corresponding roughly to the two living
groups of brittle stars: euryalid and non-euryalid ophiuroids
(Hyman, 1955; LeClair, 1996; O'Hara et al. 2017). Euryalid
ophiuroids are a clade that includes basket stars and snake
stars, encompassing less than 10% of ophiuroid taxonomic
diversity (Stöhr et al. 2012). The streptospondylous joint is a
relatively simple hourglass-shaped articulation that allows
the arm to coil with a range of motion posited to be

Fig. 1 Stereo images of 3D polygonal meshes of 24th most proximal segment of *Ophiothrix angulata* (YPM 7415), (A) distal face and (B) proximal face (see details in Table S1). The position of the dorsal ossicle mesh is tilted as the segment was rotated slightly internally during the micro-computed tomography (CT) scan; the dorsal ossicle was flat in scans of *O. angulata* where the arm was straight. Meshes visualized and imaged using Autodesk Maya (see Materials and methods).



greater than that allowed by the zygospondylous joint (Hyman, 1955; Byrne, 1994; LeClair, 1996). The streptospondylous joint is a trait that exhibits homoplasy: it is present in the Euryalida and in the non-euryalid families Ophiacanthidae and Hemieuryalidae (LeClair, 1996; Stöhr, 2012).

Non-euryalid ophiuroids, in contrast, form a polyphyletic group comprising over 90% of ophiuroid species (Stöhr et al. 2012; O'Hara et al. 2014, 2017). They show greater interspecific vertebral disparity (LeClair, 1994) and greater complexity in their vertebral articulations (LeClair, 1994; LeClair & LaBarbera, 1997), and they inhabit a greater breadth of ecological niches than the euryalids (Warner, 1982; LeClair, 1996; LeClair & LaBarbera, 1997). The zygospondylous articulation has a multifaceted process on the proximal face accommodated by a socket on the distal face (Hyman, 1955).

Two major categories of zygospondylous articulation are recognized based on morphometrics: non-keeled (Group I); and keeled (Group II; LeClair, 1994, 1996; Fig. 2). Non-keeled and keeled zygospondylous vertebrae differ in the nature of their distal and proximal processes, particularly in the presence or absence of a large keel on the distal surface of the vertebra and a corresponding groove on the aboral proximal surface (LeClair, 1996, fig. 2; Fig. 2).

The ecological and taxonomic radiation of ophiuroids has been attributed to the evolution of different vertebral joint types (Hendler & Miller, 1991; Litvinova, 1994; LeClair, 1996; LeClair & LaBarbera, 1997). Specific joint morphologies are thought to facilitate certain modes of locomotion and feeding (Hendler & Miller, 1991; LeClair & LaBarbera, 1997). These inferences rely on the assumption that vertebral morphology influences motion capabilities (Emson & Wilkie, 1982; Hendler & Miller, 1991; Litvinova, 1994). However, experimental data suggest that interspecific variation in lateral mobility is not significantly correlated with vertebral morphology or feeding ecology (LeClair & LaBarbera, 1997). Here, we use 'mobility' to refer to intersegmental range of motion; thus, 'flexibility' (sensu LeClair & LaBarbera, 1997;

Hendler & Miller, 1991) is equivalent to how we use mobility here.

The first step in addressing the larger question of the relationship between ophiuroid vertebral morphology, mobility and ecology is to evaluate functional differences between their disparate intervertebral joints. In order to build a platform to analyze the impact of vertebral morphology on the potential range of motion of the ophiuroid arm, we created 3D digital models based on micro-computed tomography (CT) scans that were used to view the relative positions of the arm ossicles during flexion. The models were validated using in vivo range of motion data from the same specimens. We used specimens of two living ophiuroids, *Ophioderma brevispina* (Say, 1825) and *Ophiothrix angulata* (Say, 1825), representing non-keeled (Group I) and keeled (Group II) zygospondylous vertebral morphologies, respectively. The analysis was conducted using zygospondylous morphologies so that disparate yet homologous morphological structures could be compared, setting up a framework that could be used to analyze the vast majority of ophiuroid vertebral disparity in future studies. This framework allows for the investigation of three hypotheses regarding the relationship between ophiuroid vertebral shape and function; we provide an initial consideration of these hypotheses here.

- 1 Range of motion does not correlate with disparity in interspecific non-euryalid vertebral morphology: In vivo behavioral observations by LeClair & LaBarbera (1997) suggested that variation in lateral mobility is not related to vertebral morphology. Our consideration of this hypothesis involved comparing the intersegmental joints during near-maximal dorsal and lateral arm flexion in two specimens each of *O. brevispina* and *O. angulata* zygospondylous vertebrae, focusing on the functional consequences of the morphological features that define vertebral groups I and II.
- 2 Mobility is inversely related to the size of the articular surfaces (the area on the distal surface of the

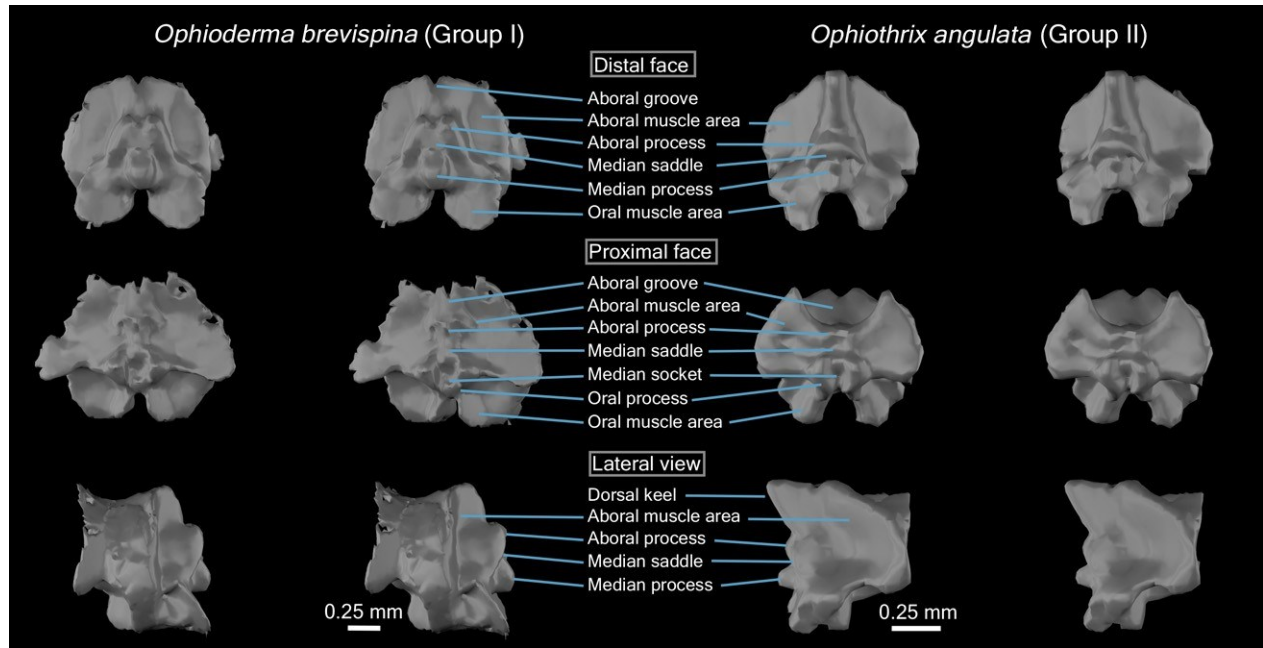


Fig. 2 Stereo images of 3D vertebral meshes showing terminology used to describe vertebral features (after LeClair, 1996, fig. 2). (A) The 11th most proximal vertebra of *Ophioderma brevispina*; (B) the 24th most proximal vertebra of *Ophiothrix angulata* (YPM 7415; see details in Table S1). Right lateral view shown in *O. brevispina*, left lateral view in *O. angulata*. Vertebral meshes visualized and imaged using Autodesk Maya.

vertebra that directly contacts the adjacent vertebra): Hendler & Miller (1991) speculated that reduced size of the articular surface of the vertebral face relative to the area of muscle insertion correlates with increased arm mobility. We provide an initial evaluation of this hypothesis by comparing near-maximal mobility in segments of the proximal and distal areas of the total free arm (by dividing the arm in two halves by length) in a specimen of *O. brevispina* [the proportion of articular surface area to surface area of the muscle insertions is relatively smaller in vertebrae of the proximal half of the arm than in those of the distal half (LeClair, 1996)].

- 3 The presence of dorsal, lateral or ventral plates reduces mobility: Litvinova (1994) regarded it as an 'obvious conclusion' that large, developed plates restrict motion of the arm. We observed the positions of these external ossicles before and during near-maximal flexion in four specimens of *O. brevispina* and *O. angulata* to determine if they are the factor-limiting range of motion in these ophiuroids.

The 3D digital models constructed here were used to document the mobility of the intervertebral joint as the arm engaged in lateral and dorsal flexion. As hypotheses of the relationship between morphology and range of motion prior to this had only been based on superficial features of isolated ossicles, we used the models to develop our understanding of the extent to which

morphological differences between ophiuroid arm segments affect function. To do so, we adapted methods used in the study of vertebrate biomechanics; this approach can be applied to the analysis of a broader range of ophiuroid taxa in the future, and to the investigation of mobility in other invertebrates.

Materials and methods

Experimental overview

We created 3D digital skeletal models of the arms of two live specimens of *O. brevispina* (Group I) and two of *O. angulata* (Group II). We used these models to observe the relative position of the ossicles during movement, and interpret how their morphology contributes to lateral and dorsal mobility. The disk diameters were 1.46 and 1.66 cm for the two specimens of *O. brevispina*, and 0.58 and 0.78 cm for the two specimens of *O. angulata*; arm length was 4.35 and 4.36 cm for *O. brevispina*, and 2.51 and 3.26 cm for *O. angulata*. Specimens were obtained from Gulf Specimen Ordering (Florida, USA). First, we measured the near-maximal range of motion of each specimen in vivo. Second, we micro-CT scanned the arms to reveal the configuration of the ossicles in this near-maximally flexed position and measured the range of motion using the digitized 3D representation of the specimen (3D volume). Third, we used nonparametric statistics to test whether the range of motion in the scan falls within that observed in vivo. Finally, we micro-CT scanned the arms in a straight position, and integrated the skeletal elements of the two scans in a 3D digital model to analyze the motion of the ossicles as they shifted from straight to flexed. All aspects of the research complied with federal

1 and Yale University protocols for working with invertebrate
2 animals.

3 4 In vivo range of motion

5 We measured the near-maximal range of dorsal and lateral arm
6 flexion in vivo in the proximal and distal halves (determined by
7 dividing the total length of the arm in half). Live animals were used
8 because measurements of museum specimens preserved in alcohol
9 might result in artifacts due to unnaturally flaccid or stiffened post
10 mortem soft tissues controlling joint motions. Dorsal and lateral
11 deviations from the straightened arm are critical directions of flexion
12 for locomotion and feeding in non-euryalid ophiuroids. The
13 term 'dorsal' here refers to direction of motion; 'aboral' is used in
14 names of morphological features (e.g. 'aboral groove', 'aboral process',
15 'aboral muscle area', etc.). The specimens were anesthetized
16 using $MgCl_2$ hexahydrate (as in Arafa et al. 2007; see also Deheyne
17 et al. 1996, 2000) by gradually increasing the concentration until
18 they became motionless and unresponsive. The proximal portion of
19 an arm was bent near-maximally in a dorsal direction from the oral
20 disk by curving the arm until it offered strong resistance. Near-maximal
21 positioning was used because measuring maximal range of
22 motion would have potentially damaged the arm ossicles, and did
23 so in some early trials with other specimens. The fragility of these
24 specimens meant that true maximal (i.e. at failure point) and near-
25 maximal motion were similarly subjective and, in our view, not far
26 apart. The specimen was braced in this position using pins and
27 photographed with a Canon Powershot G16 (12.1 megapixel) camera
28 (Fig. 3A,B). We repeated this process four times using the same arm
29 that was straightened and re-submerged in the anesthetizing
30 solution for 30 s between trials. Multiple trials were conducted to assess
31 the consistency of near-maximal flexion. The flexion of the distal
32 portion of the same arm was determined in the same way. This
33 process was repeated with a second specimen of each species to
34 measure the range of lateral motion. Only proximal flexion was
35 measured in *O. angulata*, as the arm is too small distally to allow
36 accurate data to be collected with our equipment.

37 When the in vivo flexion trials were complete, we immediately
38 micro-CT scanned each specimen with both the proximal and distal
39 portions of the arm in a near-maximally flexed position corresponding
40 to that in the in vivo measurements. The micro-CT scans were
41 obtained using the North Star Imaging ImagiX (North Star Imaging,
42 Minnesota, USA) in the Darroch Lab at Vanderbilt University (Tennessee,
43 USA; see Table S1 for scan settings and output information). Volumes
44 were reconstructed using EFX-CT software (North Star Imaging,
45 Minnesota, USA), and the micro-CT scans were visualized
46 with VG Studio MAX v. 2.2 and 3.0 software (Volume Graphics,
47 Heidelberg, Germany).

48 The 3D volume from the micro-CT scans of the specimens in near-
49 maximally flexed position provided a view equivalent to that in the
50 photographs of the in vivo trials. In every case, we measured
51 the angle formed by each segment from the photographs and from
52 the equivalent view of the 3D volume in ImageJ software (<https://imagej.nih.gov/ij/>; Fig. 3B,C). These measurements were obtained
53 to ensure that the distribution of the flexed articulations in the 3D
54 volume fell within that observed in the specimen in vivo, that is, to
55 validate the use of the scan data. We tested this by comparing the
56 distribution of flexion angles between successive segments
57 observed in vivo with those responsible for the range of motion in
58 the 3D volume. Most of the angles between successive vertebrae
59 involved in the flexion were over 6.5° in both the in vivo trials
60 and the 3D volumes; we thus considered angles of 6.5° and higher to



Fig. 3 (A, B) Setup for in vivo intersegmental angle measurement of the proximal portion of the arm of *Ophioderma brevispina*. (C) 3D volume from micro-computed tomography (CT) scan of the same specimen for comparison visualized and imaged in VG Studio MAX (see Materials and methods).

be contributing to arm flexion, and used these measurements for the analysis. Angles observed during multiple in vivo trials were pooled into a single distribution per species, arm region and type of flexion (dorsal and lateral), and compared with the distribution of angles measured in the corresponding 3D volume using a two-sample Kolmogorov–Smirnov test (Massey, 1951; Conover, 1971). This test uses the maximum difference between the cumulative density functions of the two samples as a statistic to evaluate whether both samples are drawn from a common distribution. Likewise, we tested for significant differences in the angles formed during dorsal and lateral arm flexion between: (a) specimens of the two ophiuroid species; and (b) the distal and proximal arm regions

of *O. brevispina*. In each case, values were compared using Mann-Whitney U-test. Statistical analyses were performed in the R software environment (R Core Team, 2017).

Construction of the 3D digital models

After scanning an arm in a near-maximally flexed position, we immediately straightened and re-scanned it. We used a four-step process to integrate data from the flexed and straight arms, and create the mobility models: (i) surface structure of two adjacent vertebrae were extracted as polygonal meshes from scans of straight and flexed arms; (ii) the vertebral meshes were imported into Maya software (Autodesk, San Rafael, USA; Fig. 4A); (iii) the straight and flexed orientations of the same proximal vertebral meshes were superimposed (Fig. 4B); and (iv) the location of a joint center was specified through inverse kinematics (Tolani et al. 2000; Nicolas et al. 2007) so that, when rotated, the distal ossicle from the flexed scan was superimposed on that from the straight one while minimizing overlap with the distal face of the proximal ossicle (Fig. 4C).

- 1 Extracting surface structure of two adjacent vertebrae as polygonal meshes from scans of straight and flexed arms. We extracted two articulated vertebrae from both the proximal and distal portions of the micro-CT scan of the flexed ophiuroid arm using VG Studio MAX 3.0, referred to as 'flexed proximal' and 'flexed distal', respectively. We then extracted corresponding articulated vertebrae from the scan of the straight arm ('straight proximal' and 'straight distal'; Fig. 4A).
- 2 Importing the vertebral meshes into Maya software. The four segmented vertebrae were exported from VGStudio as watertight polygonal meshes in STL format 3D image files and imported into Maya (Fig. 4A). During import and setup, we maintained the position of the vertebral meshes as they were articulated in the 3D volume (i.e. 'flexed proximal' with 'flexed distal' and 'straight proximal' with 'straight distal'). We used the articular morphology of the 'straight proximal' and 'straight distal' vertebral meshes as a neutral (or reference) pose (Gatesy et al. 2010; Fig. 5B). We assessed the joint angle and articulation of the 'flexed proximal' and 'flexed distal' vertebral meshes in reference to this neutral pose. We used this pose to compare flexion in the proximal and distal portions of the arm.
- 3 Superimposing the straight and flexed orientations of the same proximal vertebral meshes. To compare arm orientations, we superimposed the 'flexed proximal' and 'straight proximal' vertebral meshes in Maya (Fig. 4B). We added colored axes in Maya to link 'flexed proximal' and 'flexed distal' (as in Otero et al. 2017; Figs 4B and 5A). The center of each axis became a joint center with three rotational degrees of freedom: mediolateral, dorsoventral and internal/external. We designated the new joint center as the center of rotation of 'flexed distal', allowing motions in 3D to be expressed relative to the axis of rotation. The coordinate system aligned the x (red)-axis dorsoventrally so that rotation resulted in lateral flexion. The y (green)-axis was orthogonal to the x (dorsoventral)-axis. The z (blue)-axis corresponded to the longitudinal axis of the straight arm; rotations around it corresponded to internal/external rotation.
- 4 Locating the joint center. We used inverse kinematics to locate the position of the joint center along the x- and z-axes in the dorsal flexion models, and along the z-axis in the lateral flexion models. Translation along the y-axis was not considered for either dorsal or lateral flexion models, as ophiuroid

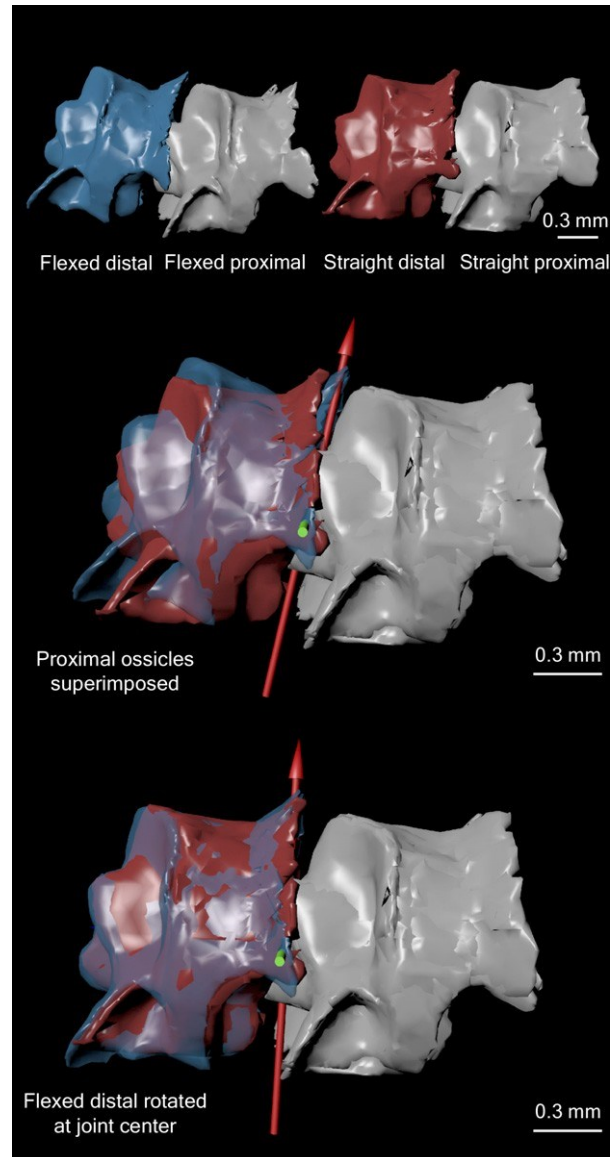


Fig. 4 Process for construction of digital models in Autodesk Maya using polygonal meshes of ophiuroid vertebrae from micro-computed tomography (CT) scans. (A) Left lateral view of vertebral meshes of *Ophioderma brevispina* (see details in Table S1). Intervertebral joint flexed dorsally (left pair) and straight (right pair). Vertebral meshes labeled as used in the text. (B) Proximal vertebral meshes superimposed for direct comparison of relative orientations of distal ossicles; 'flexed distal' at 50% transparency. Tri-colored axis inserted at joint center. (C) Joint axis rotated to superimpose distal ossicle meshes.

vertebrae are bilaterally symmetrical and all joint centers fall along the proximodistal line of symmetry. Translation along the x-axis was not considered for the lateral flexion models, as dorsoventral translation of the joint center did not affect lateral flexion. The joint center was selected as the point that optimized maximal superimposition of 'flexed distal' and 'straight distal' orientations while minimizing overlap between 'flexed distal' and 'straight proximal' ossicles. After determination and rotation of the joint center, the 'flexed distal' vertebral meshes assumed the position of 'straight distal'

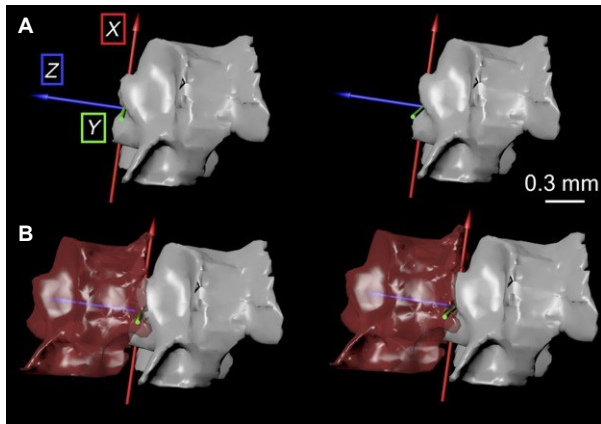


Fig. 5 Stereo images of neutral reference pose in left lateral view of vertebral mesh of *Ophioderma brevispina* visualized using Autodesk Maya (see details in Table S1) without 'straight distal' (A) and articulated with 'straight distal' at 50% transparency (B). Tri-colored axes represent coordinate system of joint center (see Materials and methods).

in the neutral reference pose (Fig. 4C). As each model focused on movement in a single plane, we used the joint center to rotate 'flexed distal' into the neutral pose of the other two planes to correct for minor rotation along the other axes. This approach allowed us to build six mobility models: dorsal flexion of: (i) the proximal and (ii) distal arms in *O. brevispina*; lateral flexion of (iii) the proximal and (iv) distal arms in *O. brevispina*; and (v) the dorsal and (vi) lateral flexions of the proximal arm in *O. angulata*.

We also assessed the shift in position of the dorsal, ventral and lateral ossicles relative to the vertebra during flexion. The five ossicles from the segments in the 'flexed distal' and 'straight distal' vertebral meshes were extracted as watertight polygonal meshes from their respective micro-CT scans and imported into a new Maya file. We maintained the position of the four non-vertebral ossicle meshes relative to their respective vertebral meshes. The vertebral mesh from the flexed scan was superimposed over that in the straight scan. The orientations of the four non-vertebral arm ossicles were compared between the two orientations.

Using digitized morphology of physical specimens

The watertight polygonal meshes used in the construction of the 3D digital models were built using an algorithm within VG Studio MAX based on the structure of the surface of a selected volume in the micro-CT scan. We noticed that reconstructing ossicle shape using this method resulted in minor differences between the shape of the meshes of the same ossicles extracted from different scans. Features of the minute ossicles in the micro-CT scans approached the size limits of the resolution of the mesh-building software. Some of the edges of the vertebrae, for example, appear rough or punctured as their width approaches this limit (e.g. Group I proximal face aboral muscle area in Fig. 2A). In addition, the close proximity of the ossicles often made it difficult to discern the outline of separate structures. Some features of the ossicles were edited after extraction, such as 2D surfaces outside the main volume of each object, but such editing was minimal in order to adhere to the original morphology as closely as possible and to minimize subjectivity.

Another artifact of micro-CT imaging is 'beam hardening', which can falsely represent the edges or relative densities of imaged objects. Acknowledging these downsides, the utility of this imaging method for studying ophiroid functional morphology significantly outweighs the shortcomings.

Ancestral state reconstruction

We performed an ancestral state reconstruction to look at the evolutionary history of Group I and Group II vertebral morphologies across Ophiuroidea. Ancestral state reconstruction was performed in R package phytools (Revell, 2012) using 100 replicates of stochastic character mapping (Bollback, 2006) under an equal rates model. The topology employed corresponded to that of O'Hara et al. (2017) with terminals pruned to the set of taxa coded by LeClair (1996).

Results

3D segment morphology

The vertebral meshes of the two taxa revealed the differences between the proximal and distal faces that distinguish the two groups of zygospondylous articulations (LeClair, 1996; Figs 2, 6 and 7). The vertebral meshes of the *O. brevispina* specimens showed the prominent proximal and distal aboral articulating processes, and the absence of a proximal aboral groove and distal keel characteristic of Group I (Figs 2A, 6A,B and 7A,B). The vertebral meshes of the *O. angulata* specimens showed the relatively reduced proximal aboral articulating process, large distal keel and proximal aboral groove characteristic of Group II (Figs 2B, 6C and 7C).

The distal aboral muscle attachments in the vertebral mesh of the Group I *O. brevispina* specimens appear relatively shallow compared with those of Group II *O. angulata* specimens in lateral view, as do the proximal aboral attachments (Fig. 8). The median process slopes gently in the *O. brevispina* specimens compared with the sharp, prominent feature in the *O. angulata* specimens (Fig. 8). We also observed notable differences in the relative size of the vertebra and the other four ossicles. The articulating surface of the vertebra adjoining the lateral ossicles is relatively larger in the *O. brevispina* specimens than in the *O. angulata* specimens. The dorsal plate extends farther beyond the proximal dorsal edge of the vertebra in the segments of *O. brevispina* than in the segments of *O. angulata*, where it rests on the vertebral keel. The vertebra does not extend distally beyond any of the other ossicles in the segments of *O. brevispina*, whereas it approaches or extends slightly beyond their distal margins in the segments of *O. angulata* (Figs 6–8).

As LeClair (1996) noted, the proximal ossicles have relatively larger aboral muscle attachment areas and smaller oral muscle attachments and articulating processes than the distal ossicles in both Group I and Group II (Fig. 6). We also

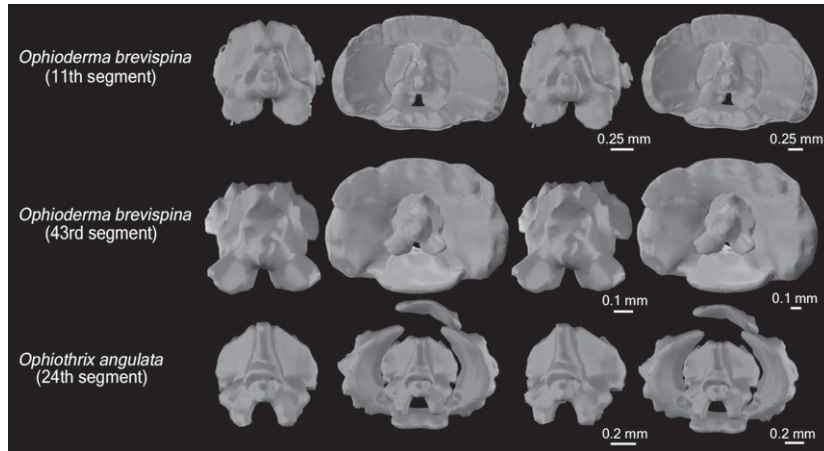


Fig. 6 Stereo images of 3D meshes of distal face of micro-computed tomography (CT) scanned ophiuroid vertebrae from (A) *Ophioderma brevispina* proximal (11th segment), (B) distal (43rd segment), and (C) *Ophiothrix angulata* (24th segment; YPM 7415). The position of the dorsal ossicle mesh in (C) is tilted as the segment was rotated slightly internally during the micro-CT scan; the dorsal ossicle was flat in scans of *O. angulata* where the arm was straight. Furthest left in row shows vertebral morphology; second to left shows vertebra articulated with non-vertebral ossicles. See Table S1 for scan and rendering details. Meshes visualized and imaged using Autodesk Maya.

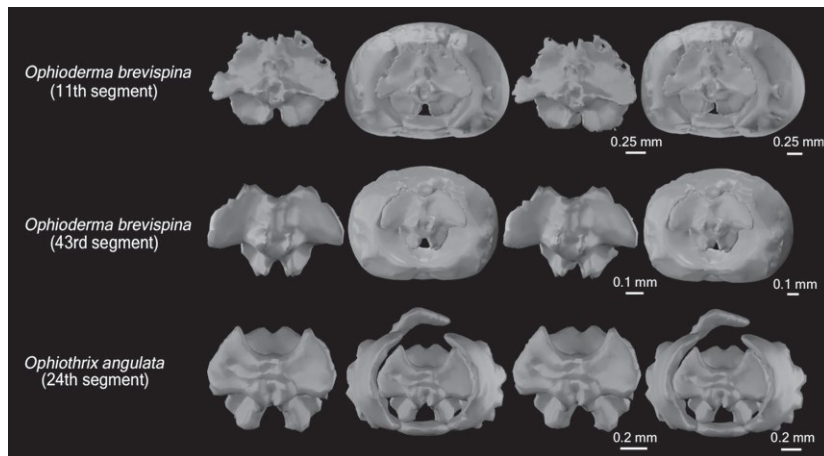


Fig. 7 Stereo images of 3D meshes of proximal face of micro-computed tomography (CT) scanned ophiuroid vertebrae from (A) *Ophioderma brevispina* proximal (11th segment), (B) distal (43rd segment), and (C) *Ophiothrix angulata* (24th segment; YPM 7415). The position of the dorsal ossicle mesh in (C) is tilted as the segment was rotated slightly internally during the micro-CT scan; the dorsal ossicle was flat in scans of *O. angulata* where the arm was straight. Furthest left in row shows vertebral morphology; second to left shows vertebra articulated with non-vertebral ossicles. See Table S1 for scan and rendering details. Meshes visualized and imaged using Autodesk Maya.

observed that the proximal vertebral meshes in the *O. brevispina* specimens (Group I) are proportionally shorter on the proximal-distal axis, have smaller articulating surfaces to the lateral ossicles (Fig. 8), and are larger dorsoventrally relative to the rest of the segment than the distal vertebral meshes (Figs 6 and 7).

Comparing range of motion measurements in vivo and with micro-CT

Angle measurements from the in vivo trials and digitized micro-CT scans can be found in Table S2. We were

unable to reject the null hypothesis that the distribution of angles obtained from the in vivo trials and the digitized micro-CT scans are drawn from the same underlying distribution in all combinations of flexion type, arm region and species (Fig. 9A–F). Overall, these results support the conclusion that the observations made using the micro-CT scan images are representative depictions of the range of motion of living specimens. We found significant differences in the angles formed by each segment in the proximal and distal portions of the arm of the *O. brevispina* specimen during both lateral and dorsal flexion (Fig. 10). Values were also significantly different

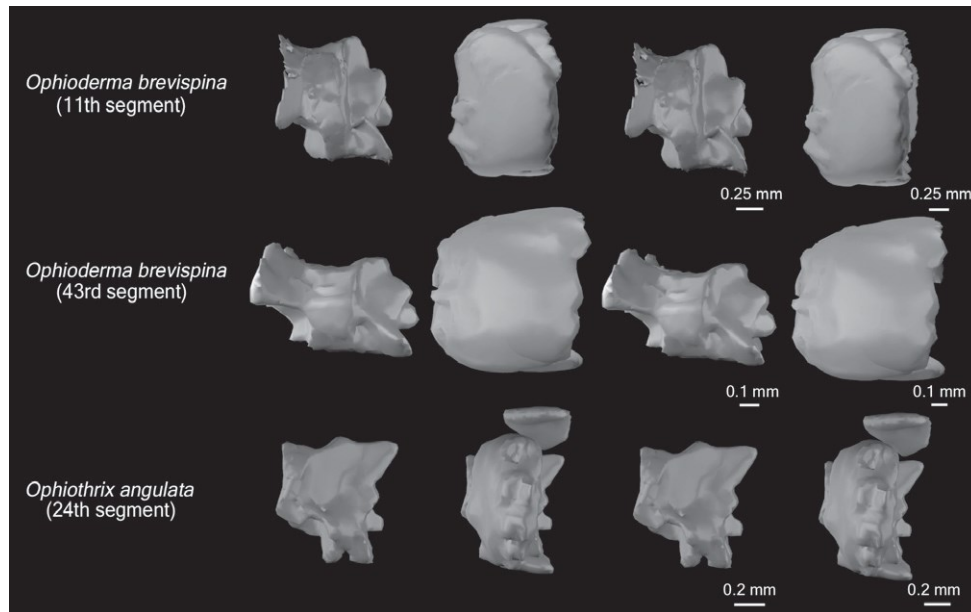


Fig. 8 Stereo images of 3D meshes of right lateral face of micro-computed tomography (CT) scanned ophiroid vertebrae from (A) *Ophioderma brevispina* proximal (11th segment), (B) distal (43rd segment), and (C) *Ophiothrix angulata* (24th segment; YPM 7415). The position of the dorsal ossicle mesh in (C) is tilted as the segment was rotated slightly internally during the micro-CT scan; the dorsal ossicle was flat in scans of *O. angulata* where the arm was straight. Furthest left in row shows vertebral morphology; second to left shows vertebra articulated with non-vertebral ossicles. See Table S1 for scan and rendering details. Meshes visualized and imaged using Autodesk Maya.

between the *O. brevispina* and *O. angulata* specimens during lateral flexion of the proximal arm region, but not during dorsal flexion of the same region.

Dorsal flexion in *Ophioderma brevispina*

Proximal vertebral ossicles

In the digital model of articulated vertebrae from the proximal half of the arm, the joint center for dorsal flexion was located on the ventral half of the median saddle on the distal face of the ossicle. During dorsal flexion, the vertebra swung out from the median process of the distal face of the adjacent vertebra and rotated towards the aboral process (Figs 2 and 11A). The distal vertebra appeared to maintain contact with portions of the median saddle, the ventral ridge of the aboral process and the dorsal side of the median process during flexion, while contact was lost between the median socket and the distal portion of the median process (Figs 2 and 11A).

Distal vertebral ossicles

In the digital model of articulated vertebrae from the distal half of the arm, the pattern of flexion was similar to that in the proximal portion of the arm. The joint center was located along the dorsal half of the median saddle, which was positioned slightly more dorsally than in the vertebrae in the proximal portion of the arm (Fig. 11B). The aboral process of the proximal face of the distal ossicle seemed to

roll more fully over the surface of the aboral process of the proximal ossicle than in the model of the proximal part of the arm.

Non-vertebral ossicles

In the proximal half of the arm, the distal end of the dorsal ossicle was lifted dorsally when the segment rotated (Fig. 12A), allowing the next segment to be rotated in turn. The lateral and ventral ossicles appeared to be rotated slightly dorsally as well (Fig. 12A). The distal non-vertebral ossicles behaved in a similar way to those in the proximal half of the arm (Fig. 12B).

Lateral flexion in *Ophioderma brevispina*

Proximal vertebral ossicles

In the digital model of articulated vertebrae from the proximal half of the arm, the joint center was located on a line passing through the median process and the bilateral plane of symmetry. The oral process/median socket glided over the median process of the adjacent vertebra. The aboral processes on the opposing faces rocked over each other about the median saddle (Figs 2 and 13A).

Distal vertebral ossicles

In the digital model of articulated vertebrae from the distal half of the arm, the joint center was located on a line passing through the distal half of the median process and the

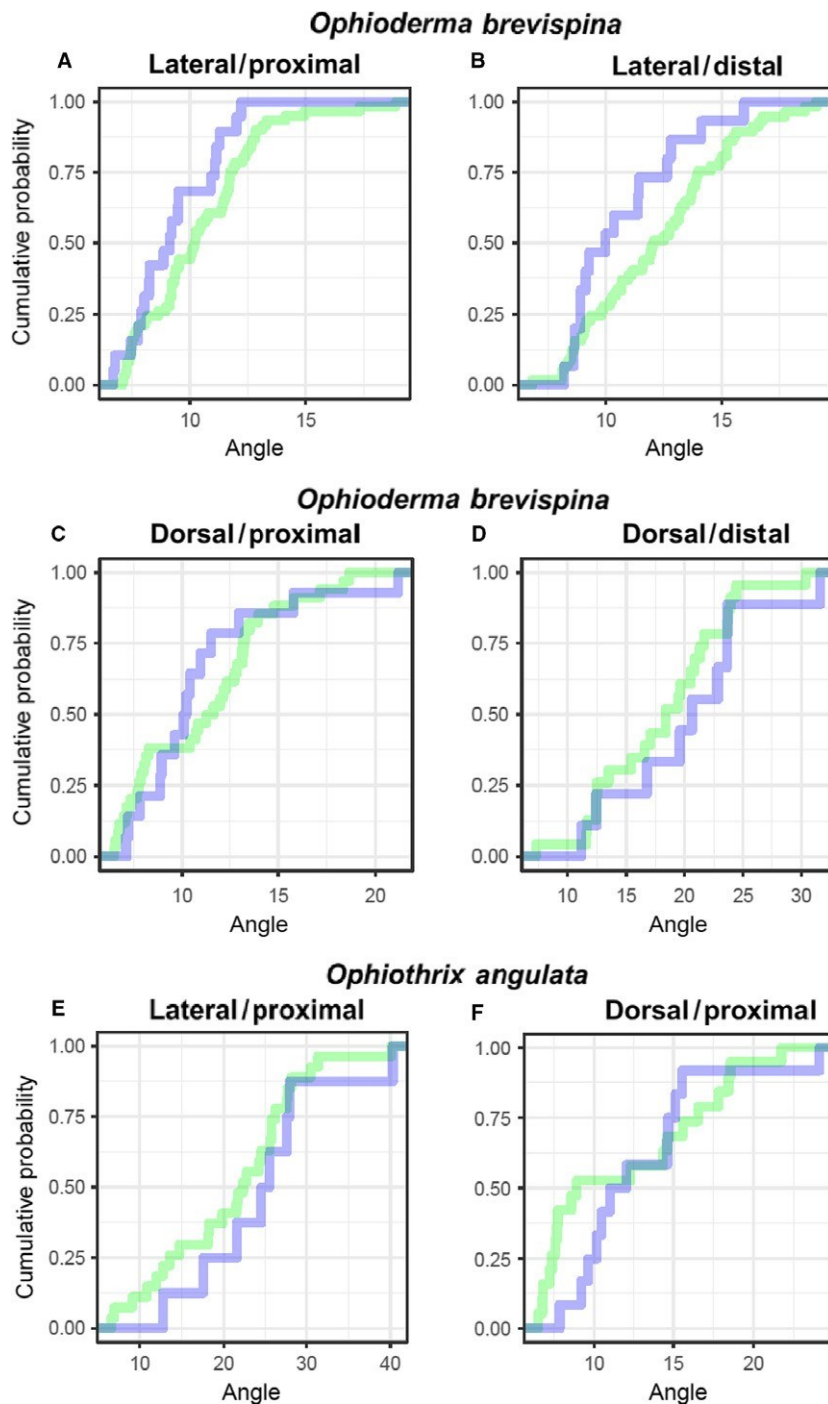


Fig. 9 Comparison of the range of motion observed in vivo and in the micro-computed tomography (CT) scan. (A–F) Cumulative density functions of joint angles formed during CT scans (blue) and in vivo assays (green). In all cases, we are unable to reject the hypothesis that both samples are drawn from the same distribution ($P = 0.15, 0.12, 0.32, 0.79, 0.73$ and 0.08 for A–F, respectively).

bilateral plane of symmetry. The distal face slid over the median saddle and rolled over the aboral process of the proximal face. The dorsal surface of the median socket glided over the dorsal surface of the median process (Fig. 13B).

Non-vertebral ossicles

The lateral ossicles rotated farther in the direction of flexion than the vertebral ossicle in the models of both the proximal and distal halves of the arm (Fig. 14A,B).

Dorsal flexion in Ophiothrix angulata

Vertebral ossicles

In the digital model of articulated vertebrae from the proximal half of the arm, the articular facet of the proximal face glided dorsally about the dorsal side of the articular facet of the adjacent ossicle (Figs 2 and 11C). The joint center was located at the center of the aboral process of the distal face; the median socket of the adjacent ossicle rotated dorsally between the dorsal area of the median process and

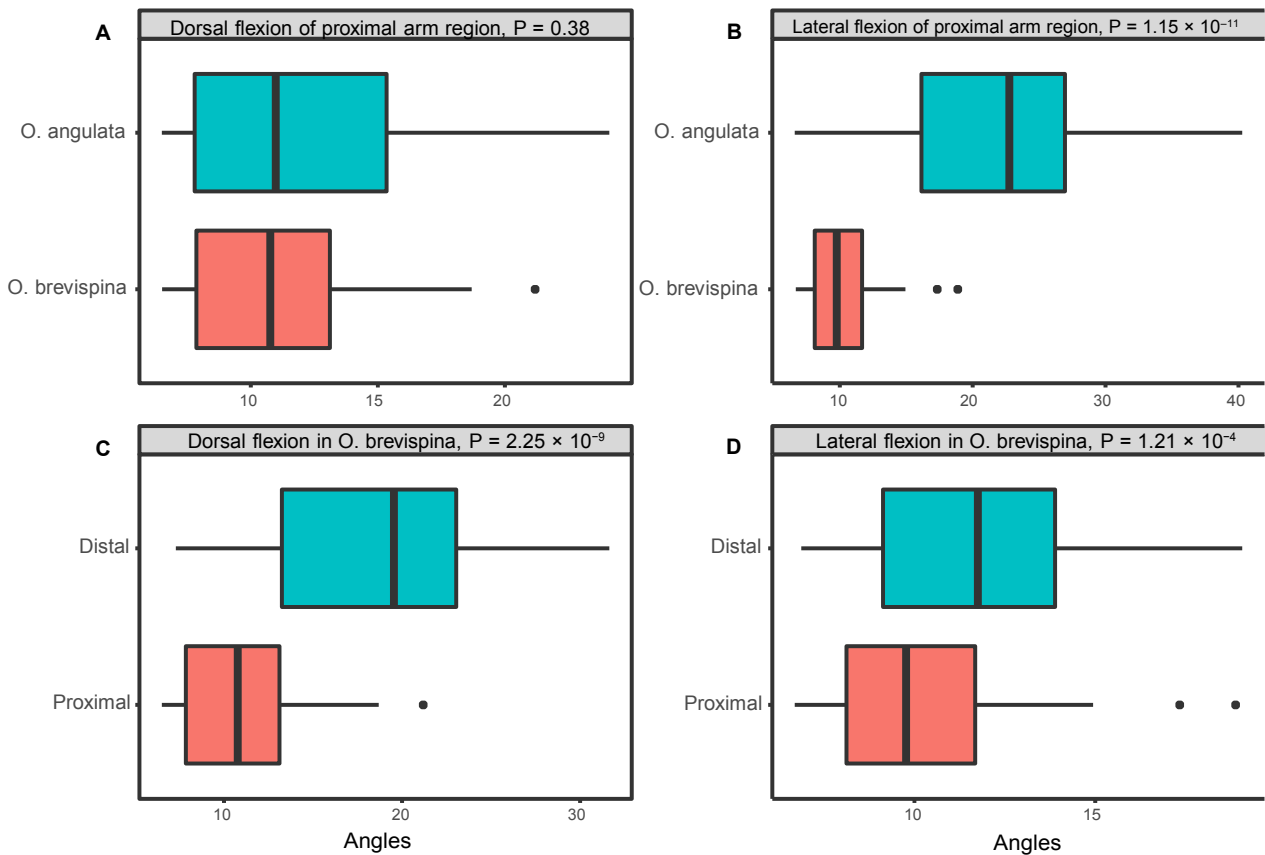


Fig. 10 Comparison of the angles formed between segments during arm flexion between species and arm regions. Values are pooled from angles taken from in vivo photographs and micro-computed tomography (CT) scans. Angles formed by the proximal part of the arms of *Ophiothrix angulata* and *Ophioderma brevispina* were significantly different during lateral flexion (B), but not during dorsal flexion (A). Differences were also significant for the proximal and distal parts of the arm during both lateral and dorsal flexion in *O. brevispina* (C,D). P-values are reported in the figure. See Table S2 for angle measurements.

the ventral area of the median saddle/aboral process on the distal face. Although this joint center was more dorsal in position on the articular facet than that in *O. brevispina*, the articular facet was more ventral in *O. angulata*, the median saddle was located deeper and the median process was more pronounced so the ossicle did not appear to swing away from the ventral half of the adjacent ossicle during dorsal flexion (Fig. 11C).

Non-vertebral ossicles

The position of the lateral and ventral ossicles remained relatively constant in the straight to flexed positions. The dorsal ossicle appeared to be raised towards the distal face of the vertebral ossicle presumably to accommodate the articulation, as it slightly overlapped the next ossicle; however, the thickness of this ossicle approached the size limits of the extraction software (Fig. 12C).

Lateral flexion in *Ophiothrix angulata*

Vertebral ossicles

In the digital model of articulated vertebrae from the proximal half of the arm, the joint center was located along a

line bisecting the center of the median process on the distal face and the bilateral line of symmetry dividing the ossicle. The median socket on the proximal face of the vertebra slid over the aboral process on the adjacent vertebra, and the dorsal part of the oral process slid over the median saddle. The proximal aboral process rolled over the distal process (Figs 2 and 13C). In near maximal flexion, the median socket was observed to rotate away from the median process, maintaining contact on the right side alone.

Non-vertebral ossicles

The lateral ossicles rotated in the same direction as the arm (Fig. 14C): when the vertebral ossicles rotated, the lateral ossicles rotated even further. This allowed the lateral ossicle on the concave side to fit between its neighboring vertebral ossicle and the lateral ossicle of the adjacent segment (Fig. 14C).

Discussion

Micro-CT scanning has been used to study brooding in extant South African brittle stars (Landschoff et al. 2015)

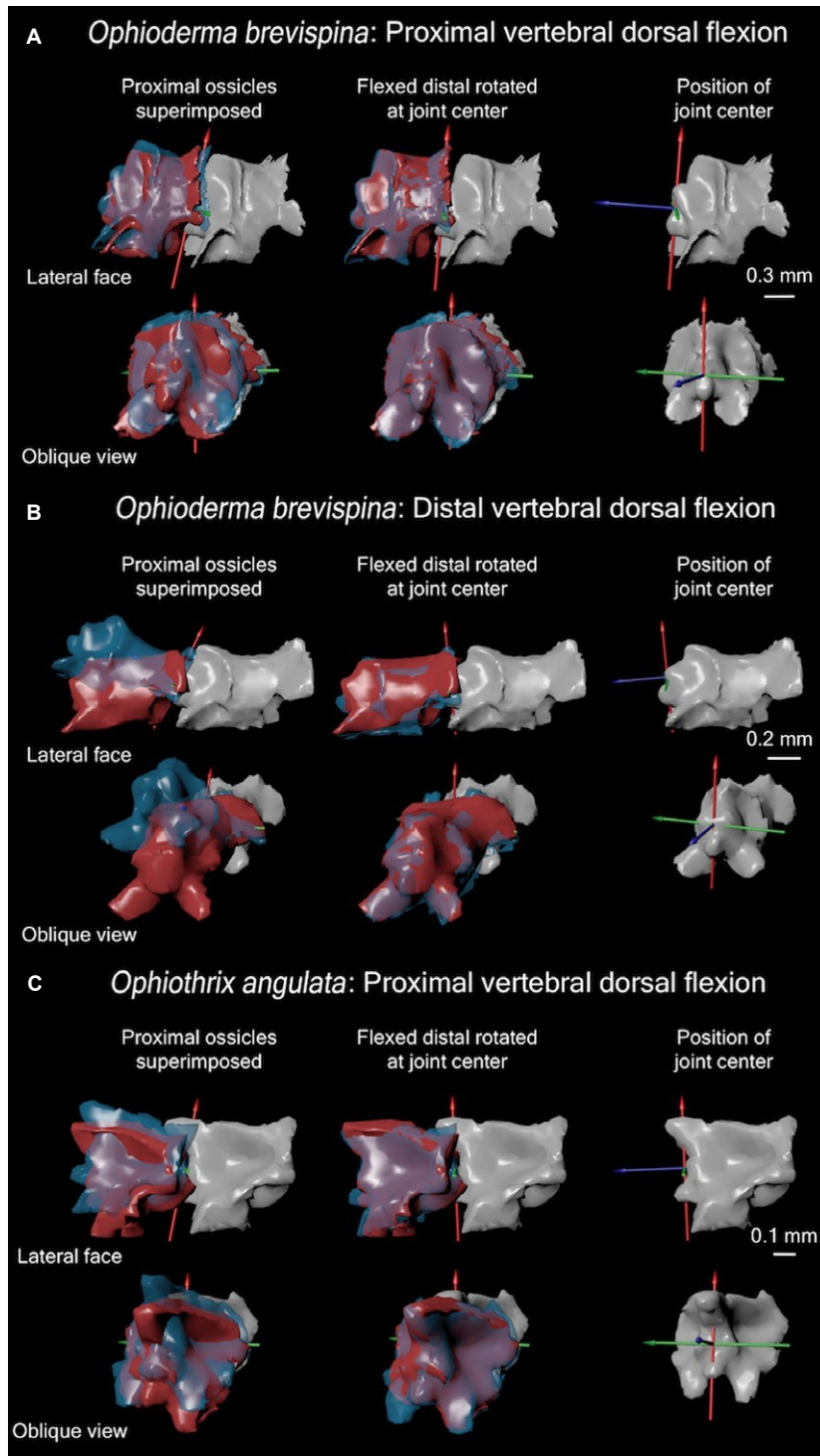


Fig. 11 Comparison of orientation of 'flexed distal' (blue) and 'straight distal' (red) vertebral meshes in left lateral and oblique views during experiment in which arm is flexed dorsally. The first column shows the original orientation of flexed distal and straight distal relative to superimposed proximal vertebra. The second column shows the degree of overlap obtained once rotated at hypothesized joint center. The third column shows the point of hypothesized joint center on distal surface of 'flexed proximal'. Ossicles are 3D meshes of micro-computed tomography (CT) scanned ophiuroid arms (see Table S1 for scan details) visualized using Autodesk Maya.

and Early Devonian fossil ophiuroids of South Africa (Reid et al. 2015). The present study, however, is the first to use digital models based on micro-CT scans for mobility analysis of the brittle star skeleton. This technique has high utility as a non-destructive tool for imaging internal ophiuroid anatomy for two main reasons. (i) micro-CT imaging makes it possible to view whole ossicles in 360° without damage.

Ophiuroid arm ossicles are very difficult to manipulate manually under a light microscope as they are often ~1 mm or less in size. Scanning electron microscopy, the typical method for viewing high-resolution morphology of the minute ossicles, leaves one side obscured, and manipulating specimens to reset them for re-imaging is very difficult. (ii) Articulations between ossicles can be observed. The

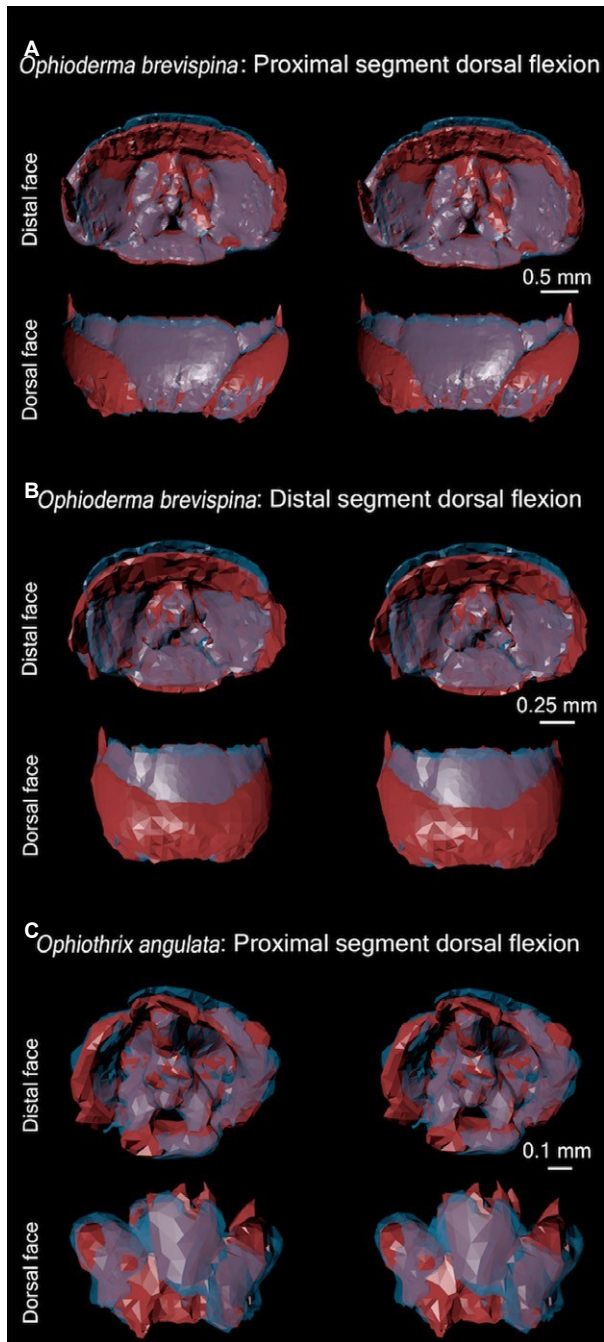


Fig. 12 Assessment of the shift in position of the dorsal, ventral and lateral ossicles relative to the vertebra during dorsal flexion. Whole segments from the 'flexed distal' (in blue) and 'straight distal' (in red; see Fig. 4A) vertebral meshes were extracted as watertight polygonal meshes from their respective micro-computed tomography (CT) scans. The vertebral meshes were superimposed to compare the relative position of the four non-vertebral arm ossicles. 3D meshes are micro-CT scanned ophiuroid arm segments (see Table S1 for scan details) visualized using Autodesk Maya. Presented as stereo images.

calcified ossicles are tightly articulated and immersed in soft tissues so the articulations both within and between segments can only be observed in full with 3D digitization.

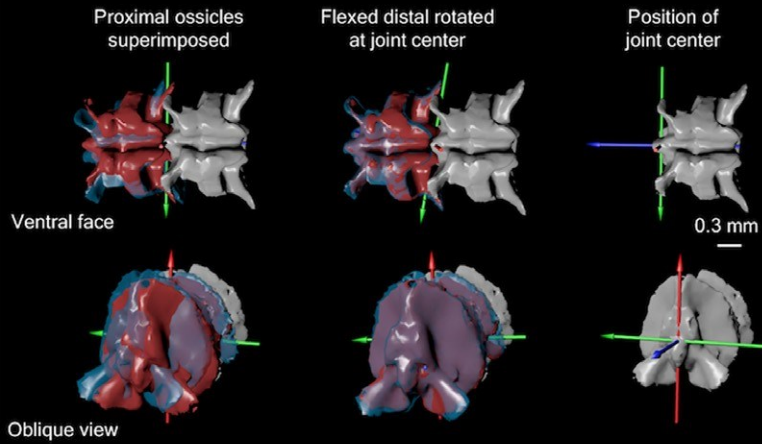
Micro-CT scanning allows for the virtual removal of soft tissues while the positions of the ossicles, as articulated in life, are maintained. This technique allowed us to view individual ossicles and their articulations in vivo in 360°. Our digital models suggest that, during dorsal flexion, the intervertebral joint center lies on the articular facet dorsally to the median process in both the specimen of *O. brevispina* (Group I) and that of *O. angulata* (Group II). The articular surface is more ventral and more deeply recessed in the *O. angulata* specimen than in the *O. brevispina* specimen. In the proximal portion of the arm of the *O. angulata* (Group II) specimen, the joint center is more deeply recessed than in that of *O. brevispina* (Group I), correlating with the relative positions of the articular surfaces. Within the articular surface, the joint center is more dorsal in position in the *O. angulata* specimen than in the *O. brevispina* specimen. During lateral flexion, the joint center is located within the median process in both the specimens of *O. angulata* and *O. brevispina*. We observed that the median socket pivoted away from the median process during maximal lateral flexion observed in the *O. angulata* specimen, extending the range of motion; however, we could not attribute this difference in function to any specific feature. Additional taxa will need to be examined to determine the range of taxa capable of this extended motion and to identify the factors responsible for this interesting aspect of lateral flexion in ophiuroids.

Our mobility models reveal differences in the mechanics of arm flexion between the specimens of the two taxa, particularly in terms of dorsal arm flexion, that seem to be directly related to their disparate vertebral morphologies. However, there were no significant differences in the angles formed during dorsal flexion of the arms of these two specimens, although the differences between them during lateral flexion were highly significant (Fig. 10). We could not identify specific morphological features responsible for these functional consequences (e.g. in the style of Hendler & Miller, 1991; Litvinova, 1994), suggesting that the factors controlling intervertebral joint function may be more complex than subtle disparities in vertebral morphology. However, the number of taxa we examined was limited; the study of articulated arm structures in additional ophiuroid taxa using the methods described here is needed to understand the relationship between form and function.

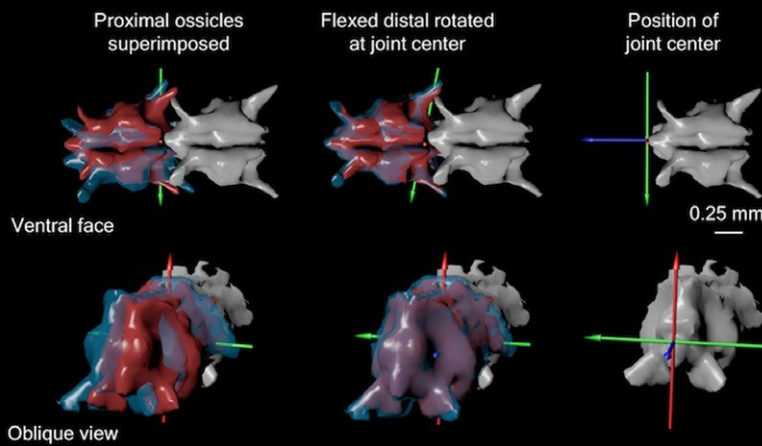
Through the observations presented, we hypothesize that interspecific disparity in vertebral morphology may be less influential in contributing to differences in range of motion than previously considered (Emson & Wilkie, 1982; Hendler & Miller, 1991; Litvinova, 1994), consistent with LeClair & LaBarbera's (1997) findings that factors influencing arm mobility in ophiuroids go beyond vertebral morphology alone. It would be necessary to integrate soft tissue and force-application capabilities into the 3D models developed here in order to identify any differences in integrated arm function between Group I and Group II. *Ophioderma*

1
2
3
4
5
6
7
8
9
10
11
12
13
14
15
16
17
18
19
20
21
22
23
24
25
26
27
28
29
30
31
32
33
34
35
36
37
38
39
40
41
42
43
44
45
46
47
48
49
50
51
52
53
54
55

A *Ophioderma brevispina*: Proximal vertebral lateral flexion



B *Ophioderma brevispina*: Distal vertebral lateral flexion



C *Ophiothrix angulata*: Proximal vertebral lateral flexion

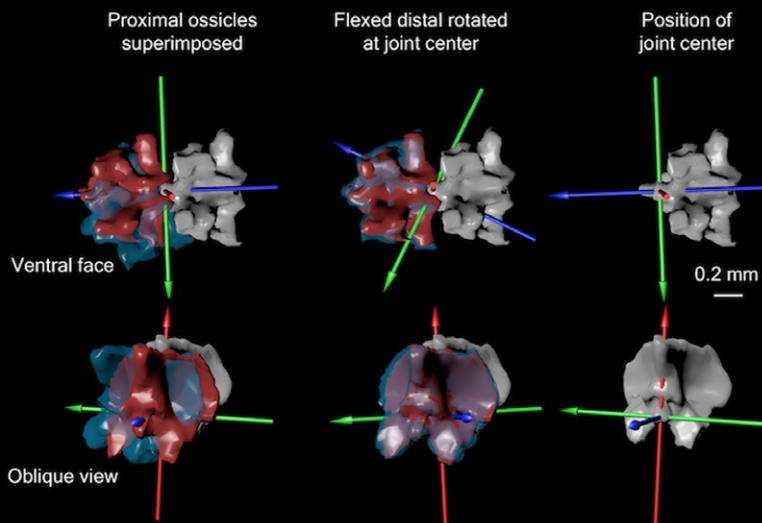


Fig. 13 Comparison of orientation of 'flexed distal' (blue) and 'straight distal' (red) vertebral meshes in ventral and oblique views during experiment in which arm is flexed laterally. The first column shows the original orientation of flexed distal and straight distal relative to superimposed proximal vertebra. The second column shows the degree of overlap obtained once rotated at hypothesized joint center. The third column shows the point of hypothesized joint center on distal surface of 'flexed proximal'. Ossicles are 3D meshes of micro-computed tomography (CT) scanned ophiuroid arms (see Table S1 for scan details) visualized using Autodesk Maya.

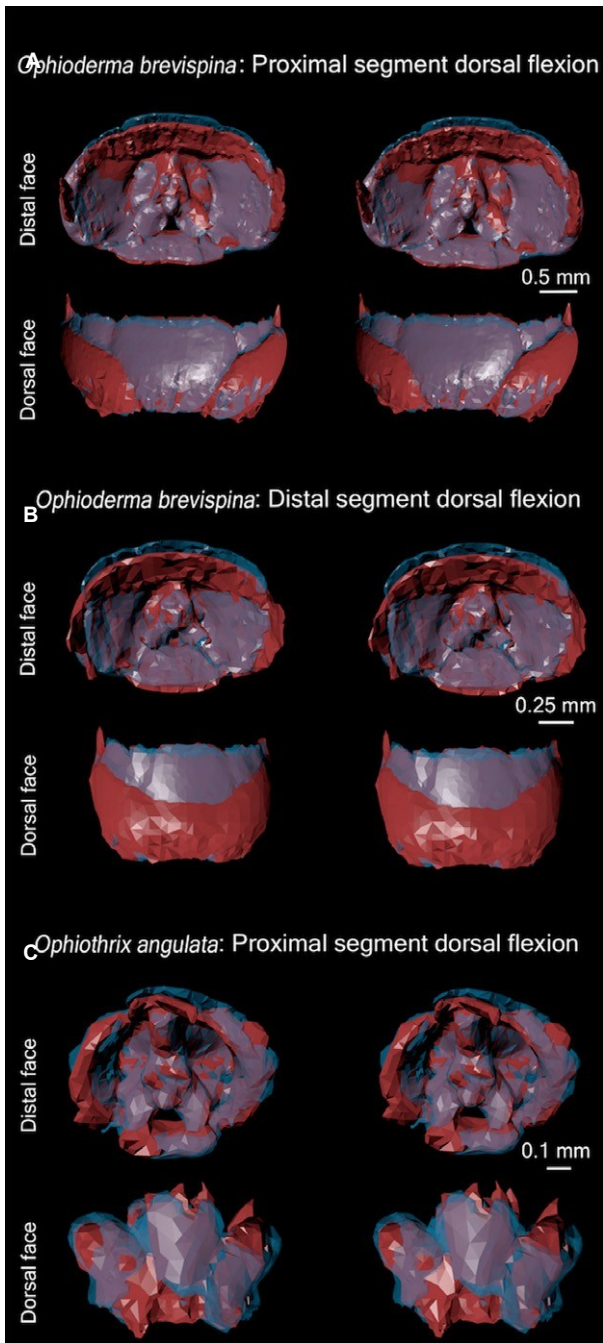


Fig. 14 Assessment of the shift in position of the dorsal, ventral and lateral ossicles relative to the vertebra during lateral flexion. Whole segments from the 'flexed distal' (in blue) and 'straight distal' (in red; see Fig. 4A) vertebral meshes were extracted as watertight polygonal meshes from their respective micro-computed tomography (CT) scans. The vertebral meshes were superimposed to compare the relative position of the four non-vertebral arm ossicles. 3D meshes are micro-CT scanned ophiuroid arm segments (see Table S1 for scan details) visualized using Autodesk Maya. Presented as stereo images.

species are known to be predators, scavengers and deposit feeders, while *Ophiothrix* species are known as primarily suspension feeders (Warner, 1982); future work will explore

the wider relationship between form and function in taxa with drastically different ecologies and day-to-day movement needs.

LeClair (1996) suggested that 'keeled vertebral ossicles are derived relative to non-keeled forms' (i.e. Group II morphology is derived relative to Group I), based on the presence of non-keeled vertebrae at the base of the arms in keeled species. Our ancestral state reconstruction confirmed that the non-keeled state represents the ancestral condition for ophiuroids, but also revealed that the keeled state is likely to have evolved convergently in two clades (Fig. 15).

The area of the articular surfaces is smaller relative to the surface area of the muscle attachment sites in vertebrae in the proximal vs. the distal portion of the arm of *O. brevispina* (LeClair, 1996); thus, Hendler & Miller's (1991) hypothesis predicts greater mobility in the proximal part of the arm. However, we found that the angles created by successive vertebrae during arm flexion were significantly smaller in the proximal arm region than in the distal one in the specimen we analyzed (Fig. 10). This seems to be related to the disparate morphologies of proximal and distal arm segments: the joint center during dorsal flexion of vertebrae in the proximal portion of the arm lies in a more ventral position on the joint interface than in those distal (represented by the tricolored axes in Fig. 11A,B). In the model constructed, the rounder, more prominent articular surface on the distal face of vertebrae in the distal portion of the arm allows the joint interface to roll over the aboral process, whereas the more flattened distal face in the proximal portion limits flexion from the joint center. During lateral flexion, the joint center for both the proximal and distal portions of the arm bisected the median process. Our observations do not support the hypothesis of Hendler & Miller (1991), as we found that a reduced articular surface decreases mobility. Analysis of additional specimens of this taxon is required to determine how widely this conclusion applies.

Other features of the arm promote greater mobility in the distal with respect to the proximal region. The flexibility of a beam composed of multiple sequential units connected by passive tissue that resists tensile forces (i.e. a multi-jointed beam) is affected by the diameter of the units and joint density (number of units per beam length; Etnier, 2001). In a multi-jointed beam, the units are connected by a relatively stiff material so that force applied is distributed across the beam; although this is not the case during normal behavior of the ophiuroid arm, in our *in vivo* trials force was distributed in such a way that each unit was flexed to its near-maximal extent. We observed an increase in mobility associated with decreased segment diameter and higher joint density within the specimen we observed of *O. brevispina*, which is to be expected if we consider the ophiuroid arm as a multi-jointed beam (Etnier, 2001). Thus, the differential mobility and flexibility within the arm observed may be

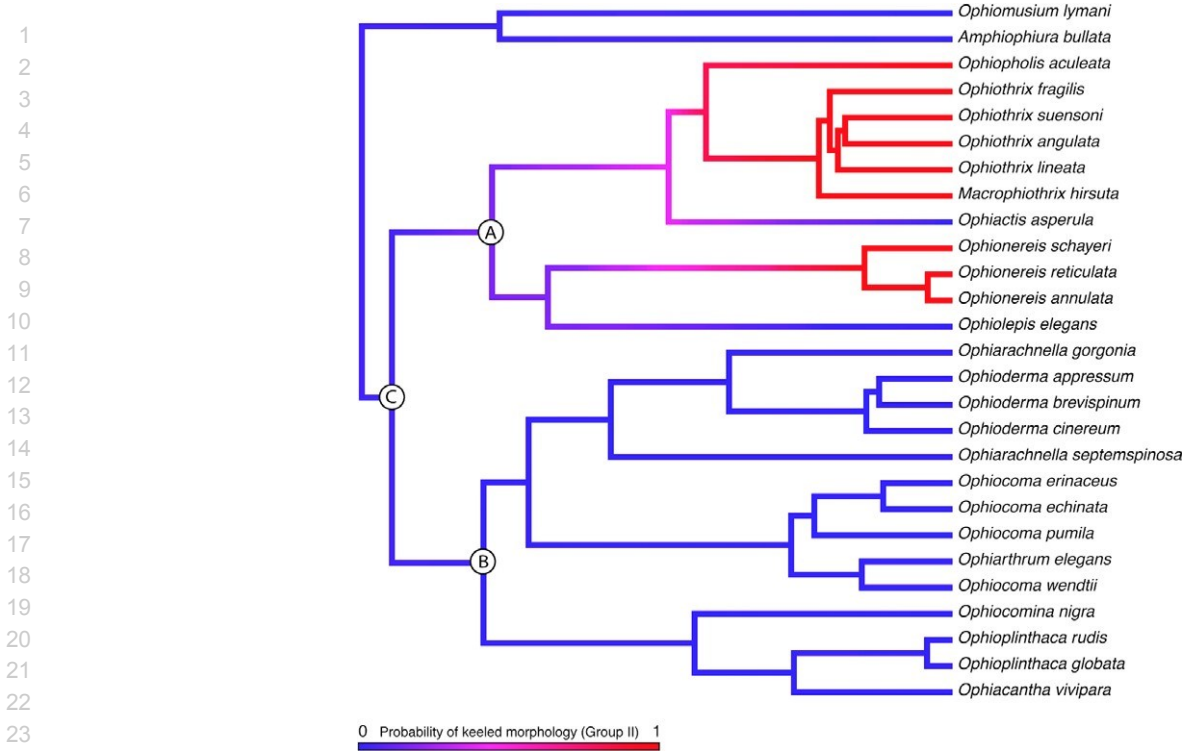


Fig. 15 Ancestral state reconstruction of the evolutionary history of ophiuroid vertebral morphologies. The topology employed corresponded to that of O'Hara et al. (2017), with terminals pruned to the set of taxa coded by LeClair (1996) as having either non-keeled (Group I) or keeled (Group II) vertebrae. Results suggest that the non-keeled vertebral morphology was present in the most recent common ancestors of Ophiuroidea, Ophintegrada (C) and the two major clades represented in our study, Amphilepidida (A) and Ophiacanthida (B). Furthermore, the keeled morphology evolved convergently at least twice within the Amphilepidida (A).

driven by the diameter and joint density along its length, as well as the ossicle morphology described.

The presence of non-vertebral arm plates might appear to inhibit flexion of the arm (Litvinova, 1994); our observations show, however, that the dorsal and lateral arm plates rotate to accommodate the changing positions of the adjacent segment during dorsal and lateral flexion, projecting further in the direction of flexion than the vertebral ossicle itself. Although further work is needed to determine the limits on the range of ophiuroid arm motion, as well as the pervasiveness of this behavior in non-vertebral plates throughout ophiuroids, our models do not support the hypothesis that non-vertebral arm plates are the limiting factor hindering flexion.

Implications

Using 3D digital modeling of ophiuroid arms built with micro-CT scan data, we identified the joint center and documented arm mobility in four specimens in order to build a framework for relating morphology to range of motion. Several aspects of our findings challenge longstanding hypotheses about ophiuroid arm mobility that were based on vertebral and arm segment morphology, and future work will expand the dataset from the two taxa examined

to investigate broad-scale patterns in the relationship between arm form and function within ophiuroids. Our results suggest that observations of ophiuroid arm morphology from isolated ossicles alone may not be sufficient for estimating functional capabilities, because the relationship between form and function among the many parts of the arm can be more complex than is easily predicted based on any single component. Further comparisons between other Group I and II species using the methods described here are required to determine the prevalence of our findings.

The morphology of lateral arm plates has been documented in terms of inter- and intra-specific disparity and relative differences along the length of the arm (Thuy & Stöhr, 2011). The functional implications of disparity in lateral arm plate morphology, and within dorsal and oral arm ossicles, could be analyzed by modifying the methods used in this study.

The evolutionary steps that resulted in the construction and locomotion capabilities of modern ophiuroid arms remain poorly understood. It has been difficult, if not impossible, to infer the movement capabilities of Paleozoic ophiuroids due to their dissimilarity to modern taxa. Movement capability is one of the most critical properties of an organism as it impacts behavioral capabilities such as

feeding and reproduction. Thus, drawing ecological inferences regarding Paleozoic taxa is contingent on understanding the mechanical abilities of their arms. It has been hypothesized that some taxa utilized tube feet for locomotion, as do modern asteroids (Glass & Blake, 2004). Determining the locomotion strategy of stem-group Paleozoic ophiuroids using the methods described herein is crucial to infer how the agile muscular-driven locomotion strategy of modern ophiuroids evolved.

This study lays the groundwork for understanding the relationship between ossicle form and function in brittle stars, and creates a framework for the analysis of movement in invertebrate groups outside the Ophiuroidea. Our results show that 3D digital models of articulated skeletal structures can reveal important information about echinoderm mobility. Thus, this method has the potential to yield important insights into the biomechanics of stem-group echinoderms, such as stylophorans (Lefebvre, 2003), shedding critical insight into the evolutionary history of deuterostome movement and locomotion.

Acknowledgements

The authors thank Rachel Racicot and Brandt Gibson (Vanderbilt University) for assistance setting up and carrying out experiments; the Structure and Motion Laboratory (Royal Veterinary College) and Steve Gatesy (Brown University) for valuable scientific discussions; Anjan Bhullar, the Bhullar Lab, Holger Petermann and the Briggs Lab (Yale University) for VG Studio support and scientific input; Aurora Krom (Duke University) for scientific input; Gulf Specimen Ordering and Yale Peabody Museum Division of Invertebrate Zoology for access to specimens; and the reviewers for their constructive feedback. Funding was provided by the Yale Peabody Museum Invertebrate Paleontology Division, the Yale University Department of Geology and Geophysics, the George Schulz Fellowship, and the Pierson College Richter Fellowship. There are no conflicts of interest.

Author contributions

J.R.H. and E.G.C. designed the experiments. E.G.C. and S.A.F.D. performed the micro-CT scans and reconstructions. N.M.K. conducted the statistical analyses. N.M.K. and E.G.C. conducted the ancestral state reconstruction. T.R.B. and S.A.S. identified structures of interest and segmented the micro-CT data with input from E.G.C. E.G.C. extracted the 3D structures and created the Maya models. E.G.C., J.R.H. and D.E.G.B. interpreted the results and prepared the manuscript with scientific and editorial input from the other authors.

References

Alexander RM (1992a) Exploring Biomechanics: Animals in Motion. New York: Scientific American Library.

- Alexander RM (ed.) (1992b) Comparative and Environmental Physiology 11: Mechanics of Animal Locomotion. Berlin: Springer.
- Alexander RM (2003) Principles of Animal Locomotion. Princeton: Princeton University Press.
- Arafa S, Sadok S, El Abed A (2007) Assessment of magnesium chloride as an anaesthetic for adult sea urchins (*Paracentrotus lividus*): incidence on mortality and spawning. *Aquac Res* 38, 1673–1678.
- Arshavskii YI, Kashin SM, Litvinova NM, et al. (1976a) Coordination of arm movement during locomotion in ophiurans. *Neurophysiology* 8, 404–410.
- Arshavskii YI, Kashin SM, Litvinova NM, et al. (1976b) Types of locomotion in ophiurans. *Neurophysiology* 8, 398–404.
- Astley HC (2012) Getting around when you're round: quantitative analysis of the locomotion of the blunt-spined brittle star, *Ophiocoma echinata*. *J Exp Biol* 215, 1923–1929.
- Barbaglio A, Tricarico S, Ribeiro A, et al. (2012) The mechanically adaptive connective tissue of echinoderms: its potential for bio-innovation in applied technology and ecology. *Mar Environ Res* 76, 108–113.
- Barbaglio A, Tricarico S, Di Benedetto C, et al. (2013) The smart connective tissue of echinoderms: a materializing promise for biotech applications. *Cah Biol Mar* 54, 713–720.
- Baumiller TK, Messing CG (2007) Stalked crinoid locomotion, and its ecological and evolutionary implications. *Palaeontologia Electronica* 10, 1–10.
- Bels VL, Gasc J-P, Casinos A (eds) (2003) Vertebrate Biomechanics and Evolution. Oxford: BIOS Scientific Publishers.
- Bisby FA, Roskov Y, Orrell T, et al. ((2010) Species 2000 & ITIS Catalogue of Life: 2010 Annual Checklist. Digital resource at <http://www.catalogueoflife.org/annual-checklist/2010>. Species 2000: Reading, UK.
- Brusca RC, Brusca GJ (1990) Invertebrates, 2nd edn. Sunderland: Sinauer Associates.
- Byrne M (1994) Ophiuroidea. In: *Microscopic Anatomy of the Invertebrates*, Vol. 14. (eds Harrison FW, Chia F-S), pp. 247–343. New York: Wiley-Liss.
- Candia Carnevali MD, Burighel P (2010) Regeneration in echinoderms and ascidians. In: *Encyclopedia of Life Sciences (ELS)*. (ed. ????) pp. ????. Chichester: John Wiley.
- Clark EG, Bhullar B-AS, Darroch SAF, et al. (2017) Water vascular system architecture in an Ordovician ophiuroid. *Biol Lett* 13, 1–5.
- Conover WJ (1971) *Practical Nonparametric Statistics*. New York: Wiley.
- Deheyn D, Alva V, Jangoux M (1996) Fine structure of the photogenous areas in the bioluminescent ophiuroid *Amphipholis squamata* (Echinodermata, Ophiuroidea). *Zoomorphology* 116, 195–204.
- Deheyn D, Malfet J, Jangoux M (2000) Cytological changes during bioluminescence production in dissociated photocytes from the ophiuroid *Amphipholis squamata* (Echinodermata). *Cell Tissue Res* 299, 115–128.
- Domenici P, González-Calderón D, Ferrari RS (2003) Locomotor performance in the sea urchin *Paracentrotus lividus*. *J Mar Biol Assoc UK* 83, 285–292.
- Dupont S, Thorndyke M (2007) Bridging the regeneration gap: insights from echinoderm models. *Nat Rev Genet* 8,
- Edgecombe GD, Giribet G, Dunn CW, et al. (2011) Higher-level metazoan relationships: recent progress and remaining questions. *Organ Divers Evol* 11, 151–172.
- Emson RH, Wilkie IC (1982) The arm-coiling response of *Amphipholis squamata* (Delle Chiaje). In: *Echinoderms: Proceedings*

- 1 of the International Conference, Tampa Bay. (ed. Lawrence
2 JM), pp. 11–18. Rotterdam: A. A. Balkema.
- 3 Etnier SA (2001) Flexural and torsional stiffness in multi-jointed
4 biological beams. *Biol Bull* 200, 1–8.
- 5 Gatesy SM, Baier DB, Jenkins FA, et al. (2010) Scientific roto-
6 scoping: a morphology-based method of 3-D motion analysis
7 and visualization. *J Exp Zool* 313A, 244–261.
- 8 Gebruk A (1995) Locomotory organs in the elasipodid holothuri-
9 ans: functional-morphological and evolutionary approaches.
10 In: *Echinoderm Research 1995*. (eds Emson RH, Smith AB,
11 Campbell AC), pp. 95–102. Rotterdam: A. A. Balkema.
- 12 Glass A, Blake DB (2004) Preservation of tube feet in an ophi-
13 uroid (Echinodermata) from the Lower Devonian Hunsrück
14 Slate of Germany and a redescription of *Bundenbachia bene-
15 ckei* and *Palaeophiomys grandis*. *Paläontologische Zeitschrift*
16 78, 73–95.
- 17 Glynn PW (1965) Active movements and other aspects of the
18 biology of *Astichopus* and *Leptosynapta* (Holothuroidea). *Biol*
19 *Bull* 129, 106–127.
- 20 Green DW, Ben-Nissan B, Yoon K-S, et al. (2016) Bioinspired
21 materials for regenerative medicine: going beyond the human
22 archetypes. *J Mater Chem B* 4, 2396–2406.
- 23 Halanych KM (2004) The new view of animal phylogeny. *Annu*
24 *Rev Ecol Evol Syst* 35, 229–256.
- 25 Hansen B (1972) Photographic evidence of a unique type of
26 walking in deep-sea holothurians. *Deep-Sea Res* 19, 461–462.
- 27 Hendler G, Miller JE (1991) Swimming ophiuroids – real and
28 imagined. In: *Biology of Echinodermata, Proceedings of the*
29 *Seventh International Echinoderm Conference*. (eds Yanagi-
30 sawa T, Yasumasu I, Oguro C, Suzuki N, Motokawa T), pp.
31 179–190. Rotterdam: A.A. Balkema.
- 32 Hyman LH (1955) *The Invertebrates: Echinodermata*, Vol. IV.
33 New York: McGraw-Hill.
- 34 Kano T, Suzuki S, Watanabe W, et al. (2012) Ophiuroid robot
35 that self-organizes periodic and non-periodic arm movements.
36 *Bioinspir Biomim* 7, 1–8.
- 37 Kano T, Sato E, Ono T, et al. (2017) A brittle star-like robot cap-
38 able of immediately adapting to unexpected physical damage.
39 *Royal Soc Open Sci* 4, 1–14.
- 40 Kerkut GA (1953) The forces exerted by the tube feet of the
41 starfish during locomotion. *J Exp Biol* 30, 575–583.
- 42 Lake JA (1990) Origin of the Metazoa. *PNAS* 87, 763–766.
- 43 Lal SP, Yamada K, Endo S (2008) Emergent motion characteristics
44 of a modular robot through genetic algorithm. In: *Advanced*
45 *Intelligent Computing Theories and Applications, 4th Interna-
46 tional Conference on Intelligent Computing*. (eds Huang D-S,
47 Wunsch DC, Levine DS, Jo K-H), pp. 225–234. Berlin: Springer.
- 48 Landschoff J, Plessis AD, Griffiths CL (2015) A dataset describing
49 brooding in three species of South African brittle stars, com-
50 prising seven high-resolution, micro X-ray computed tomogra-
51 phy scans. *GigaScience* 4, 1–3.
- 52 Leach DH, Dagg AI (1983) A review of research on equine loco-
53 motion and biomechanics. *Equine Vet J* 15, 93–102.
- 54 LeClair EE (1994) Quantitative morphological variation in the
55 vertebral ossicles of the Ophiuræ (Ophiuroidea). In: *Echino-
derms Through Time: Proceedings of the Eighth International*
Echinoderm Conference. (eds David B, Guille A, Féral J-P, Roux M), pp. 443–448. Rotterdam: A. A. Balkema.
- LeClair EE (1996) Arm joint articulations in the ophiuran brit-
tlestars (Echinodermata: Ophiuroidea): a morphometric analy-
sis of ontogenetic, serial, and interspecific variation. *J Zool*
240, 245–275.
- LeClair EE, LaBarbera MC (1997) An in vivo comparative study of
intersegmental flexibility in the ophiuroid arm. *The Biological*
Bulletin 193, 77–89.
- Lefebvre B (2003) Functional morphology of stylophoran echin-
oderms. *Palaeontology* 46, 511–555.
- Litvinova NM (1994) The life forms of ophiuroidea (based on
the morphological structures of their arms). In: *Echinoderms*
*through Time: Proceedings of the Eight International Echino-
derm Conference*. (eds David B, Guille A, Féral J-P, Roux M),
pp. 449–454. Rotterdam: A. A. Balkema.
- Mao S, Dong E, Jin H, et al. (2014) Gait study and pattern gen-
eration of a starfish-like soft robot with flexible rays actuated
by SMAs. *J Bionic Eng* 11, 400–411.
- Massey FJ Jr (1951) The Kolmogorov-Smirnov Test for Goodness
of Fit. *J Am Stat Assoc* 46, 68–78.
- Matsuzaka Y, Sato E, Kano T, et al. (2017) Non-centralized
and functionally localized nervous system of ophiuroids: evi-
dence from topical anesthetic experiments. *Biol Open* 6,
425–438.
- Moore AR (1924) The nervous mechanism of coordination in the
crinoid, *Antedon rosaceus*. *J Gen Physiol* 6, 281–288.
- Nicolas G, Multon F, Berillon G, et al. (2007) From bone to plau-
sible bipedal locomotion using inverse kinematics. *J Biomech*
40, 1048–1057.
- O'Hara TD, Hugall AF, Thuy B, et al. (2014) Phylogenomic reso-
lution of the Class Ophiuroidea unlocks a global microfossil
record. *Curr Biol* 24, 1874–1879.
- O'Hara TD, Hugall AF, Thuy B, et al. (2017) Restructuring higher
taxonomy using broad-scale phylogenomics: the living Ophi-
uroidea. *Mol Phylogenet Evol* 107, 415–430.
- Ohta S (1985) Photographic observations of the swimming
behavior of the deep-sea pelagothuriid holothurian *Enypni-
astes* (Elasipoda, Holothuroidea). *J Oceanogr Soc Jpn* 41, 121–
133.
- Otero A, Allen V, Pol D, et al. (2017) Forelimb muscle and joint
actions in Archosauria: insights from *Crocodylus johnstoni*
(Pseudosuchia) and *Mussaurus patagonicus* (Sauropodomor-
pha). *PeerJ* 5, e3976.
- Pawson DL (2007) Phylum Echinodermata. *Zootaxa* 1668, 749–
764.
- R Core Team (2017) R: A language and environment for statisti-
cal computing. R Foundation for Statistical Computing,
Vienna, Austria. URL <https://www.R-project.org/>
- Reid M, Bordy EM, Taylor W (2015) Taphonomy and sedimentol-
ogy of an echinoderm obrution bed in the Lower Devonian
Voorstehoek formation (Bokkeveld Group, Cape Supergroup)
of South Africa. *J Afr Earth Sc* 110, 135–149.
- Say T (1825) On the species of the Linnaean genus *Asterias*
inhabiting the coast of the U.S. *J Acad Nat Sci Phil* 5, 141–154.
- Shaw GD, Fontaine AR (1990) The locomotion of the comatulid
Florometra serratissima (Echinodermata: Crinoidea) and its
adaptive significance. *Can J Zool* 68, 942–950.
- Smith JE (1947) The activities of the tube feet of *Asterias rubens*
L. I. The mechanics of movement and of posture. *J Cell Sci* 88,
1–14.
- Stöhr S (2012) Ophiuroid (Echinodermata) systematics – where
do we come from, where do we stand and where should we
go? *Zoosymposia* 7, 147–161.
- Stöhr S, O'Hara TD, Thuy B (2012) Global diversity of brittle
stars (Echinodermata: Ophiuroidea). *PLoS ONE* 7, 3.
- Thuy B, Stöhr S (2011) Lateral arm plate morphology in brittle
stars (Echinodermata: Ophiuroidea): new perspectives for

1 ophiuroid micropalaeontology and classification. *Zootaxa*
2 3013, 1–47.
3 Tolani D, Goswami A, Badler NI (2000) Real-time inverse kine-
4 matics techniques for anthropomorphic limbs. *Graph Models*
5 62, 353–388.
6 Warner G (1982) Food and feeding mechanisms: Ophiuroidea.
7 In: *Echinoderm Nutrition*. (eds Jangoux M, Lawrence JM), pp.
8 161–181. Rotterdam: A. A. Balkema.
9 Watanabe W, Kano T, Suzuki S, et al. (2012) A decentralized
10 control scheme for orchestrating versatile arm movements in
11 ophiuroid omnidirectional locomotion. *J R Soc Interface* 9,
12 102–109.
13 Wilkie IC (1978a) Functional morphology of the autotomy plane
14 of the brittlestar *Ophiocomina nigra* (Abildgaard) (Ophi-
15 uroidea, Echinodermata). *Zoomorphologie* 91, 289–305.
16 Wilkie IC (1978b) Arm autotomy in brittle stars (Echinodermata:
17 Ophiuroidea). *J Zool* 186, 311–330.

18 Wilkie IC (2005) Mutable collagenous tissue: overview and
19 biotechnological perspective. In: *Progress in Molecular and*
20 *Subcellular Biology (Marine Molecular Biotechnology)* 39. (ed.
21 Mantranga V), pp. 221–250. Berlin: Springer.
22 Wilt FH (2005) Developmental biology meets materials science:
23 morphogenesis of biomineralized structures. *Dev Biol* 280, 15–
24 25.

Supporting Information

Additional Supporting Information may be found online in the Supporting Information section at the end of the article:

Table S1. Settings and output information from the micro-CT scanning conducted in this investigation.

Table S2. Joint angle measurements of flexed ophiuroid arms from the in vivo trials and digital micro-CT scans.

1
2
3
4
5
6
7
8
9
10
11
12
13
14
15
16
17
18
19
20
21
22
23
24
25
26
27
28
29
30
31
32
33
34
35
36
37
38
39
40
41
42
43
44
45
46
47
48
49
50
51
52
53
54
55